On the Cross-Layer Network Planning for Flexible Ethernet over Elastic Optical Networks

Hui Liang, Nelson L. S. da Fonseca, and Zuqing Zhu, *Senior Member, IEEE*

***Abstract*—This paper studies the cross-layer network planning that tries to combine flexible Ethernet (FlexE) and elastic optical networks (EONs), for FlexE-over-EONs. We focus our investigation on the most challenging setting, *i.e.*, the FlexE-over-EONs based on the FlexE-aware architecture, and consider both single-hop and multi-hop scenarios for the cross-layer planning. For the single-hop scenario, we assume that all the client flows are routed over end-to-end lightpaths in the EON. We formulate a mixed integer linear programming (MILP) model for this problem, transform it into the class constrained bin packing problem (CCBP), and leverage the primal-dual interior-point (PDIP) method to propose a polynomial-time approximation algorithm for it. Then, for the multi-hop scenario, we use a more realistic assumption that each client flow can be routed over multiple lightpaths in the EON. We show that after solving the virtual topology design, the cross-layer planning in this scenario can be transformed into that in the single-hop scenario. Therefore, an integer linear programming (ILP) model is formulated to tackle the virtual topology design, and we design a polynomial-time approximation algorithm for it by modifying the well-known branch-and-bond method. To evaluate the performance of our two-step method for the multi-hop scenario, we also propose a heuristic algorithm. Extensive simulations verify that regarding large-scale cross-layer planning for FlexE-over-EONs, our approximation algorithms are significantly more time-efficient than the ILP/MILP models, and their solutions have bounded gaps to the optimal ones and are much better than those of the heuristic.**

***Index Terms*—Flexible Ethernet (FlexE), Elastic optical networks (EONs), Approximation algorithms, Traffic grooming.**

I. Introduction

RECENTLY, fast development of datacenter (DC) and metro networks are happening all over the world, to adapt to the raising of 5G, cloud computing, and Big Data analytics [1–5]. This has imposed intensive pressure on networking technologies, especially for Ethernet and optical transport network (OTN). We have witnessed promising advances in these two areas over the past decade, to address the increasing challenges. For instance, Flex Ethernet (FlexE) [6] has been published by the Optical Internetworking Forum (OIF), which defines new Ethernet connection types to allow DC operators to utilize OTN bandwidth in more flexible manners, and provides the interface techniques for realizing service isolation and network sharding.

The major advantage of FlexE is that it leverages time-division multiplexing (TDM) to support a variety of media access control (MAC) rates that may or may not correspond to any existing physical channel (PHY) rates of Ethernet [7]. As the most recent implementation agreement, FlexE 2.0 [7] promises to be capable of carrying the collections of 100 GbE, 200 GbE, and 400 GbE PHYs. The upcoming FlexE 2.1 will add the support for 50 GbE PHYs. With these PHYs, FlexE can support various MAC rates with the operation principle shown in Fig. 1. Specifically, FlexE inserts a shim layer in between the MAC and physical layers, which divides the bandwidth resources in a group of PHYs into a series of calendar slots (CS'), and maps the data streams from FlexE clients whose data-rates can be various to the CS'. In other words, the shim layer schedules to transmit the client data from MAC interfaces with different rates in the CS' (*i.e.*, the transmission opportunities in the PHYs based on TDM).

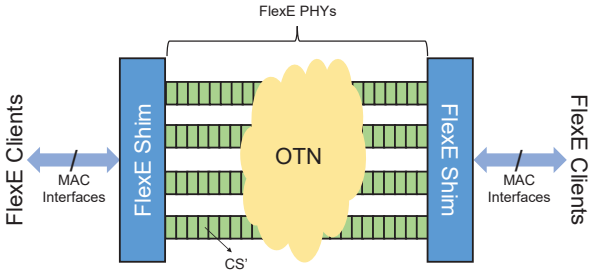

Fig. 1. Generic operation principle of FlexE.

As the data-rates of the MAC interfaces and PHYs can be different, FlexE utilizes three mechanisms [7]: 1) bonding, *e.g.*, supporting a 200 Gbps MAC interface with two bonded 100 GbE PHYs, 2) sub-rating, *e.g.*, transmitting the data from a 50 Gbps MAC over a 100 GbE PHY, and 3) channelization, *e.g*, supporting a 150 Gbps and two 25 Gbps MAC interfaces with two bonded 100 GbE PHYs. Hence, even though FlexE allocates bandwidth in terms of exclusive time slots, it still has the advantage of high efficiency due to statistical multiplexing.

Meanwhile, for long distance transmissions, the data carried by FlexE PHYs needs to be further fed into the transport boxes (T-Boxes) in an OTN [8]. Therefore, the network planning for FlexE-over-OTN is an interesting but challenging problem to investigate, because it actually involves sophisticated cross-layer mapping, *i.e.*, MAC interfaces to FlexE PHYs, and FlexE PHYs to T-Boxes. Depending on how well the T-Boxes are compatible with FlexE, FlexE-over-OTN can be built with three architectures, *i.e.*, the FlexE-unaware, FlexE-partially-aware, and FlexE-aware ones, respectively [7]. Among them, only the FlexE-aware architecture uses the T-Boxes that are fully compatible with FlexE, *i.e.*, each of them equips a FlexE

H. Liang and Z. Zhu are with the School of Information Science and Technology, University of Science and Technology of China, Hefei, Anhui 230027, P. R. China (email: zqzhu@ieee.org).

N. Fonseca is with the Institute of Computing, State University of Campinas, Campinas, SP 13083-852, Brazil.

Manuscript received on May 5, 2020.

shim layer to recognize the data from each MAC interface in PHYs. Hence, the network planning for it has the most flexible cross-layer mapping, which can provide the best performance in terms of resource utilization and cost-effectiveness. On the other hand, its network planning is also most challenging because the cross-layer mapping has the maximized flexibility.

Previously, Eira *et al.* [9] has performed a thoughtful comparative analysis on architecting FlexE-over-OTNs using fixed-grid wavelength-division multiplexing (WDM) networks (*i.e.*, FlexE-over-WDMs) with the three architectures mentioned above. However, they did not consider the flexible-grid elastic optical networks (EONs) [10–14]. EONs leverage bandwidth-variable transponders (BV-Ts) and bandwidth-variable wavelength-selective switches (BV-WSS') to realize OTNs with fine spectrum allocation granularities at 12.5 GHz or even narrower. Meanwhile, with sliceable BV-Ts [15–17], one can utilize the split-spectrum scheme [18–20] to change the data-rates of a T-Box at will. To this end, we expect that an EON-based OTN would be much more friendly toward FlexE.

In [21], we studied how much exactly FlexE and EON can benefit each other mutually, and considered the three FlexE-over-OTN architectures (*i.e.*, the FlexE-unaware, FlexE-partially-aware, and FlexE-aware ones) to confirm the benefits of FlexE-over-EON over FlexE-over-WDM. Nevertheless, the problem of cross-layer network planning for FlexE-over-EONs has not been fully explored in [21]. This is because we used an impractical assumption that all the traffic flows from MAC interfaces are routed over end-to-end lightpaths in the EON, and only formulated mixed integer linear programming (MILP) models that will be intractable for large-scale problems. Note that, the cross-layer planning problems for FlexE-over-WDMs and FlexE-over-EONs are not fundamentally different from the mathematical perspective. The study in [21] has already shown that by restricting the values of certain variables to different ranges, a same MILP model can address both FlexE-over-WDMs and FlexE-over-EONs. However, in a FlexE-over-EON, the BV-Ts can take much more line-rates than those in a FlexE-over-WDM. Hence, the solution space of the cross-layer planning in a FlexE-over-EON is much larger, which makes the problem harder to be solved with good performance.

In this paper, we tackle the problem of cross-layer network planning for FlexE-over-EONs, and focus our problem-solving on the most challenging setting, *i.e.*, the FlexE-over-EONs based on the FlexE-aware architecture. We first consider a simple "single-hop" scenario, where all the traffic flows from MAC interfaces are still assumed to be routed over end-to-end lightpaths in the EON. We prove that the cross-layer planning for this single-hop scenario can be transformed into the class constrained bin packing problem (CCBP) [22], and leverage the primal-dual interior-point (PDIP) method [23] to design a polynomial-time approximation algorithm for solving it.

Next, we expand our study to consider a more realistic multi-hop scenario, where each traffic flow from MAC interfaces can be routed over multiple lightpaths in the EON [24, 25]. We first formulate an integer linear programming (ILP) model to tackle the virtual topology design in it, and then propose a polynomial-time approximation algorithm by modifying the well-known branch-and-bond method [26]. After solving the virtual topology design in the multi-hop scenario, we obtain the hop-by-hop lightpath routing of each traffic flow from MAC interfaces, and thus transform the cross-layer planning to that of the single-hop scenario. To measure the performance of our two-step method for the multi-hop scenario, we also propose a heuristic algorithm. Finally, we run extensive simulations to evaluate our proposals, and the results confirm that regarding large-scale cross-layer planning for FlexE-over-EONs, our approximation algorithms outperform the ILP/MILP models significantly in terms of running time, and their solutions are much better than those of the heuristic.

The rest of the paper is organized as follows. Section II provides a brief survey on the related work. We describe the network model in Section III. The algorithm designs for the single-hop and multi-hop scenarios are discussed in Sections IV and V, respectively. We present simulation results in Section VI. Finally, Section VII summarizes the paper.

II. Related Work

Ethernet is a successful technology that has proven its efficiency in interconnecting network elements and carrying IP traffic in access and metro networks. However, when it comes to covering relatively large geographical areas, Ethernet needs the assistance from OTN to overcome physical-layer impairments [27]. Hence, Ethernet-over-OTN has become a common practice in metro and core networks. Nevertheless, traditional Ethernet interfaces were not developed on account of the standard data-rates in OTN. The introduction of FlexE resolves this mismatch [6], and thus FlexE-over-OTN can deliver improved efficiency and flexibility. On the other hand, to accommodate the dynamic traffic from Ethernet, OTN should be able to allocate bandwidth in a sub-wavelength granularity and not be restricted by the fixed wavelength grids [28], which can be realized with EONs. Therefore, Flex and EON can benefit each other mutually, and we expect that the deployment of FlexE-over-EONs in future Internet will help operators realize effective traffic grooming and scheduling optimization, and thus both the capital expenditure (CAPEX) and the operating expense (OPEX) can be greatly reduced [9, 21]. Last but not least, the bandwidth allocation mechanism of FlexE makes it easier to slice virtual networks in a FlexE-over-EON [6], while virtual network slicing is an important technique to improve the resource utilization and cost-effectiveness in today's core and metro networks [29–31].

FlexE-over-EON is essentially one type of packet-over-EONs. As a packet-over-EON consists of both packet and optical layers, the network planning and service provisioning in it need to consider the multilayer scenario. Specifically, its operator needs to address at least two tasks, *i.e.*, the virtual topology design and traffic grooming. The virtual topology design is for the operator to establish lightpaths in the optical layer to layout the virtual links for supporting the traffic matrix of the packet layer, and it needs to solve the famous routing and spectrum assignment (RSA) problem [32–37]. The traffic grooming is to groom and route packet flows over the virtual links (*i.e.*, the lightpaths) [38, 39]. Previously, considering different network environment and optimization

objective, the studies in [38–42] have formulated various ILP/MILP models and designed numerous heuristic algorithms to address the network planning and service provisioning in packet-over-EONs. However, none of these studies have considered FlexE-over-EONs, and because they did not take the special features of FlexE into account, their approaches can hardly be leveraged to solve the cross-layer network planning for FlexE-over-EONs, especially for the traffic grooming part.

For the problem of traffic grooming in packet-over-EONs, the most well-known approach is based on the auxiliary graphs (AGs) [43–46]. Zhang *et al.* [43] proposed a three-layer AG model to address the mixed-electrical-optical grooming in packet-over-EONs under a dynamic traffic scenario. Also considering dynamic service provisioning, the study in [44] addressed the mixed channel traffic grooming in a shared backup path protected packet-over-EON and designed an AG-based heuristic to solve the problem. The authors of [45] formulated an ILP model to fully explore the adaptivity of packet-over-EONs for multilayer restoration, and they also proposed an AG-based heuristic to reduce the time complexity of network planning. In [46], energy-efficient traffic grooming has been tackled in consideration of different kinds of BV-Ts and traffic scenarios. Nevertheless, all these studies did not address FlexE-over-EONs either, and they relied on ILP/MILP models and heuristics to solve the problem of traffic grooming, which either will become intractable for large-scale problems or cannot provide approximation solutions whose gaps to the optimal ones are bounded.

The architectural advantages of FlexE-over-OTNs have been analyzed in [47, 48]. However, they only performed conceptual analysis but did not address the actual problem of cross-layer network planning. The cross-layer planning of FlexE-over-OTNs was first considered in [49], but the authors relied on the assumption that T-Boxes do not have FlexE-awareness, *i.e.*, the FlexE-partially-aware and FlexE-aware architectures were not addressed. The study in [50] was the first one that comprehensively accounted the FlexE-unaware, FlexE-partially-aware, and FlexE-aware architectures and investigated the cross-layer planning in them. Later on, the authors extended their work in [9], where they formulated ILP models and designed greedy-based heuristics to solve the cross-layer planning. Nevertheless, since the heuristics are not approximation algorithms, they cannot get the solutions whose performance gaps to the optimal ones are bounded. Moreover, the studies in [9, 50] did not consider FlexE-over-EONs. In [21], we formulated MILP models to optimize the cross-layer planning in FlexE-over-EONs and utilized their results to demonstrate the benefits of FlexE-over-EONs over FlexE-over-WDMs. However, the problem-solving did not use realistic assumptions or consider the designs of approximation algorithms. Therefore, to the best of our knowledge, this is the first study that tackles the cross-layer planning in FlexE-over-EONs with in-depth theoretical analysis and approximation algorithm designs.

III. Problem Description

In this section, we first explain the operation principle of FlexE-over-EONs in the FlexE-aware architecture, and then describe the network model for cross-layer planning.

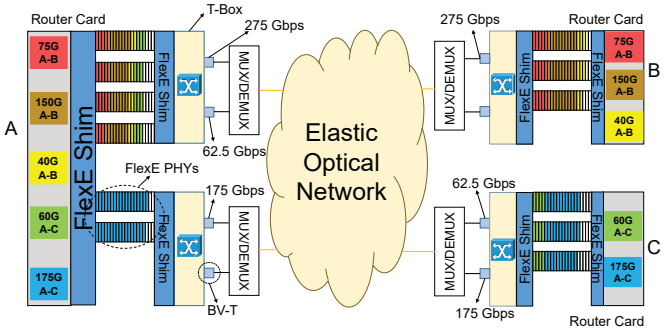

Fig. 2. Example on FlexE-over-EON in the FlexE-aware architecture.

A. Operation Principle

Similar to the FlexE-over-WDMs discussed in [9], FlexE-over-EONs can also be realized based on the FlexE-unaware, FlexE-partially-aware, and FlexE-aware architectures. In the FlexE-unaware architecture, the connections between PHYs and BV-Ts are preset and the BV-Ts have to use a fixed data-rate, while in the FlexE-partially-aware architecture, the BV-Ts can adjust their data-rates according to the usage of the CS' in PHYs. Note that, in these two architectures, only the router cards possess FlexE shims, and this limits their flexibility. On the other hand, the T-Boxes in the FlexE-aware architecture are equipped with FlexE shims, which can recognize the data from each MAC interface in the PHYs, and thus flow-level routing can be realized through the T-Boxes [7, 9]. In other words, the FlexE-aware architecture places FlexE shims not only between the MAC interfaces and PHYs but also between the PHYs and T-Boxes. Hence, instead of directly mapping PHYs to the BV-Ts in each T-Box, the architecture can sort out the data in each PHY and map it to the BV-Ts accordingly. Our analysis in [21] has already verified that the FlexE-aware architecture is the most flexible and promising one for realizing FlexE-over-EONs. Therefore, this work only considers the FlexE-aware architecture for the cross-layer planning of FlexE-over-EONs.

Fig. 2 shows an example on the FlexE-over-EON in the FlexE-aware architecture. Note that, the overall architectures of FlexE-over-EONs and FlexE-over-WDMs are very similar, except for that FlexE-over-EONs are equipped with BV-Ts. Hence, Fig. 2 is adapted from the FlexE-over-WDM in the FlexE-aware architecture in [9]. There are three nodes (*i.e.*, *Nodes* A-C) in the FlexE-over-EON, and the colored boxes in the router card of each node represent the flows from/to the MAC interfaces of its FlexE clients. For the FlexE-over-EON, the cross-layer planning assigns flows from MAC clients to one or more T-Boxes through the PHYs connected to them, and then the flows will be transmitted with the CS' in these PHYs, which is realized by leveraging the bonding, sub-rating and channelization mechanisms of FlexE [7]. Next, because each T-Box can identify the flows in the PHYs connected to it, the cross-layer planning also lets it serve flows with its BV-Ts according to the flows' destinations.

For instance, if we assume that the total capacity of a T-Box is 400 Gbps and the capacity of each BV-T in a T-Box can be adjusted with a granularity of 12.5 Gpbs, the flows from *Node* A to *Nodes* B and C can be planned as illustrated in

Fig. 2. Specifically, the cross-layer planning is conducted as follows. We first map the top four flows in *Node* A to the PHYs that connects to its first T-Box. Among the four flows, the first three are all for A-B and their total capacity is 265 Gbps. This means that they can be sent out through the first BV-T with the rate of 275 Gbps (*i.e.*, corresponding to 22 frequency slots (FS') in the EON, if an FS is assumed to provide a capacity of 12.5 Gbps). Then, the remaining capacity in the first T-box is 125 Gbps, which can only accommodate the fourth flow (*i.e.*, A-C at 60 Gbps). This is the reason why we only allocate the top four flows to the first T-Box in *Node* A. The second BV-T in the first T-Box uses a capacity of 62.5 Gbps to send the fourth flow to *Node* C, while the last flow is transmitted through the first BV-T in the second T-Box.

B. Network Model

With the aforementioned example, we can see that regarding the cross-layer network planning for FlexE-over-EON in the FlexE-aware architecture, two mappings need to be solved, *i.e.*, flows from the MAC interfaces of FlexE clients to FlexE PHYs, and FlexE PHYs to T-Boxes. The two mappings are correlated with each other, and they are both restricted by the working principle of FlexE-over-EONs. Therefore, the cross-layer planning is a complex problem to solve.

As shown in Fig. 2, each node in a FlexE-over-EON consists of router cards (on the FlexE side) and T-Boxes (on the EON side). We assume that each node equips with a fixed number of router cards, and each router card can send data through P PHYs and use them to connect to T T-Boxes. Note that, due to the restrictions from hardware complexity and cost, a T-Box usually only possesses a small number of BV-Ts [46], each of which can only set up one lightpath to a destination. However, the flows to a router card can choose arbitrary nodes in the network as destinations. Hence, if we want to ensure the the flexibility of FlexE-over-EONs, it is reasonable to assume that the flows to one router card will be served by multiple T-Boxes, *i.e.*, the capacity of a router card is larger than that of a T-Box, and this is also the case in practical implementations [7, 9]. Each router card needs to serve a few client flows from its MAC interfaces, while the client flows can have different bandwidth requirements and destination nodes. Each T-Box consists of B BV-Ts. We assume that the BV-Ts in each T-Box are sliceable BV-Ts [15, 17], which means that the capacity of a BV-T can be adjusted with a granularity of 12.5 Gbps and the total capacity of all the BV-Ts in a T-Box is fixed.

Regarding the network planning in the EON, we consider two scenarios, *i.e.*, the single-hop and multi-hop ones. The single-hop scenario assumes that the client flows are transmitted all-optically end-to-end in the EON. In other words, if a client flow is mapped to a BV-T in one T-Box, the lightpath from the BV-T will be ended at the flow's destination node without any optical-to-electrical-to-optical (O/E/O) conversions in between. The single-hop scenario over-simplifies the network planning, and thus we also consider the multi-hop scenario in which each client flow can be routed over multiple lightpaths with O/E/O conversions and de-/re-grooming in intermediate nodes. Here, the O/E/O conversions are introduced to move the client flows between the EON and FlexE layers, but they are not for bypassing the spectrum continuity constraint on lightpaths. Hence, whether they cause wavelength conversions or not is irrelevant to our problem solving. Actually, the key problem in the multi-hop scenario is the virtual topology design, *i.e.*, how to plan the lightpaths to carry all the client flows with multi-hop routing. This is because after getting the virtual topology, we transform the network planning into that in the single-hop scenario.

For both scenarios, the cross-layer planning tries to minimize the number of T-Boxes used to carry the client flows. Since previous studies have already addressed the RSA in EONs intensively, we would not explicitly solve it in our cross-layer planning. Specifically, after the lightpaths have been planned, their RSA schemes can be obtained by leveraging an existing algorithm (*e.g.*, the fragmentation-aware approaches in [12, 34, 51]). Note that, the problem considered in this work is for static network planning, which means that it needs to be solved before a network operator actually builds its FlexE-over-EON. Therefore, similar to other studies on EON planning (*e.g.*, in [32]), we assume that the optical spectra in the EON will always be sufficient to support all the lightpaths, and all the client flows will be served. To ensure this assumption is practical, we can analyze the capacity of fiber links in the EON and limit the maximum number of T-Boxes per node accordingly. This makes our network model consider the fiber capacity constraints implicitly. In our future work, we will address the cases in which request blocking will occur due to insufficient fiber capacity.

IV. Single-Hop Scenario

In this section, we design algorithms to solve the cross-layer network planning in the single-hop scenario. We first formulate an MILP model [21] to describe the optimization, leverage it to transform the cross-layer planning to the class constrained bin packing problem (CCBP) [22], and then propose a polynomial-time approximation algorithm for it. We also design a greedy-based heuristic, which can be used as the benchmark for the performance comparisons related to large-scale problems.

A. MILP Model

The following MILP model describe the cross-layer planning for a FlexE-over-EON in the FlexE-aware architecture.

Notations:

- $G(V, E)$: the FlexE-over-EON's physical topology, where V and E are the sets of nodes and fiber links, respectively.
- R: the set of client flows, where r_i is the i-th client flow, which has a bandwidth demand of w_i in Gbps and the source-destination pair as s_i-d_i.
- P: the number of PHYs that each router card can use.
- T: the number of T-Boxes that each router card can use.
- B: the number of BV-Ts in each T-Box.
- K_v: the set of router cards in node v, where $k \in K_v$ refers to such a router card.
- B_v: the set of BV-Ts in node v, where $b \in B_v$ refers to such a BV-T (*i.e.*, its T-Box and router card are denoted as $t_{v,b}$ and $k_{v,b}$, respectively).

- $B_{v,t}$: the set of BV-Ts in T-Box t of node v.
- $T_{v,k}$: the set of T-Boxes that the router card k in node v can use, where $t \in T_{v,k}$ refers to such a T-Box.
- C_p: the capacity of a PHY in Gbps ($C_p = 100$ Gbps).
- C_g: the capacity granularity of a BV-T ($C_g = 12.5$ Gbps).

Variables:

- $\alpha_{i,b}$: the boolean variable that equals 1 if client flow $r_i \in R$ is transmitted via BV-T b in node s_i, and 0 otherwise.
- $\beta_{v,k}$: the boolean variable that equals 1 if router card k in node v is used, and 0 otherwise.
- $\beta_{v,b}$: the boolean variable that equals 1 if BV-T b in node v is used, and 0 otherwise.
- $\beta_{v,t}$: the boolean variable that equals 1 if T-Box t in node v is used, and 0 otherwise.
- $p_{v,b}$: the nonnegative variable that indicates the used capacity of BV-T b in node v (*i.e.*, in terms of C_g).
- a_v: the nonnegative integer variable that indicates the number of used router cards in node v.
- b_v: the nonnegative integer variable that indicates the number of used T-Boxes in node v.
- c_v: the nonnegative integer variable that indicates the number of used BV-Ts in node v.

Objective:

The optimization objective is to minimize the total number of T-Boxes used in the cross-layer network planning.

$$\text{Minimize} \quad \sum_{v \in V} b_v. \tag{1}$$

Constraints:

$$\sum_{b \in B_{s_i}} \alpha_{i,b} = 1, \quad \forall r_i \in R. \tag{2}$$

Eq. (2) ensures that each flow r_i is transmitted via one and only one BV-T in its source node s_i.

$$\begin{aligned} &\alpha_{i,b} + \alpha_{j,b} \le \beta_{v,b}, \quad \forall v \in V,\ b \in B_v, \\ &\{i,j : r_i, r_j \in R,\ s_i = s_j = v,\ d_i \ne d_j\}. \end{aligned} \tag{3}$$

Eq. (3) ensures that a BV-T b in node v can only carry the client flows whose destination nodes are the same.

$$\sum_{\{i: r_i \in R,\ s_i = v\}} \alpha_{i,b} \cdot w_i \le p_{v,b} \cdot C_g, \quad \forall v \in V,\ b \in B_v. \tag{4}$$

Eq. (4) ensures that the total bandwidth of all the client flows assigned to each BV-T b does not exceed the BV-T's capacity, where w_i is the bandwidth demand of the i-th client flow.

$$\begin{aligned} &\sum_{b \in B_{v,t}} \sum_{\{i: r_i \in R,\ s_i = v\}} \alpha_{i,b} \cdot w_i \le \frac{C_p \cdot P}{T}, \\ &\forall v \in V,\ k \in K_v,\ t \in T_{v,k}. \end{aligned} \tag{5}$$

Eq. (5) ensures that the total bandwidth of all the client flows assigned to each T-Box t does not exceed the T-Box's capacity.

$$\beta_{v,b} \le \beta_{v,k_{v,b}}, \quad \forall v \in V,\ b \in B_v. \tag{6}$$

Eq. (6) ensures that when a BV-T b in node v is used, the corresponding router card is also marked as used.

$$\beta_{v,b} \le \beta_{v,t_{v,b}}, \quad \forall v \in V,\ b \in B_v. \tag{7}$$

Eq. (7) ensures that when a BV-T b in node v is used, the corresponding T-Box is also marked as used.

$$\sum_{k \in K_v} \beta_{v,k} \le a_v, \quad \forall v \in V, \tag{8}$$

$$\sum_{k \in K_v} \sum_{t \in T_t} \beta_{v,t} \le b_v, \quad \forall v \in V, \tag{9}$$

$$\sum_{b \in B_v} \beta_{v,b} \le c_v, \quad \forall v \in V. \tag{10}$$

Eqs. (8)-(10) ensure that the values of a_v, b_v, and c_v are correctly set, respectively.

Lemma 1. *The cross-layer network planning modeled with the MILP above can be transformed into a general case of CCBP, and thus it is an $\mathcal{NP}$-hard problem.*

Proof: First of all, we can easily verify that in the single-hop scenario, minimizing the total number of used T-Boxes is equivalent to minimizing the number of T-Boxes used in each node. Therefore, we decompose the optimization in the MILP into $|V|$ independent subproblems. For the subproblem about node $v \in V$, we treat all the client flows that originate from node v as items, each of which has a size of w_i (*i.e.*, the bandwidth demand) and a color class d_i (*i.e.*, the destination node). Each T-Box in node v is treated as a bin whose size capacity is $\frac{C_p \cdot P}{T}$, and it can accommodate items with B (*i.e.*, the number of BV-Ts in each T-Box) color classes at most. Then, we transform the subproblem into a general case of CCBP [22]. Hence, the cross-layer network planning can be transformed into a general case of CCBP. As CCBP is an $\mathcal{NP}$-hard problem, we also prove its $\mathcal{NP}$-hardness. ■

B. Approximation Algorithm Design

Since the cross-layer planning for FlexE-over-EONs is $\mathcal{NP}$-hard, we will not try to design exact algorithms for it but decide to propose a polynomial-time approximation algorithm. The main idea of the approximation algorithm is to classify flows into different types based on their bandwidth demands and process the flows in the same type similarly, and thus the time complexity can be significantly reduced compared to solving the MILP directly. Meanwhile, as the problem can be transformed into CCBP, we can leverage the primary-dual interior point (PDIP) method [23] to develop the approximation algorithm. *Algorithm* 1 shows the overall procedure. Here, we need to obtain the capacity of each T-Box as an input, *i.e.*,

$$C_{\max} = \frac{C_p \cdot P}{T}. \tag{11}$$

The for-loop checks each node $v \in V$ and minimizes the number of used T-Boxes in it in each iteration (*Lines* 1-8). Here, *Lines* 2-3 are for the initialization, and we define the size of each flow as its normalized bandwidth demand[1]. Then, *Line* 4 uses *Algorithm* 2 to classify flows in R_v into small, medium, and largest ones according to the flows' sizes and the preset tolerance ε. Next, we construct a linear programming (LP) to

[1]Note that, the normalization in *Line* 3 is just for the convenience of choosing the value of ε and classifying the flows accordingly, but it is not mandatory, *i.e.*, *Algorithm* 1 can operate without it.

serve the medium flows and utilize *Algorithm* 3 to solve it with the PDIP method (*Line* 5). Finally, we serve the small and largest flows with *Algorithm* 4 and obtain the number of used T-Boxes in node v (*Lines* 6-7). In *Line* 9, after checking all the nodes in V, we return the total number of used T-Boxes.

Algorithm 1: Overall Procedure of PDIP-based Approximation Algorithm

Input: Physical topology $G(V, E)$, set of client flows R, capacity of a T-Box $C_{\max}$, and tolerance ε.
Output: Total number of used T-Boxes.

1 **for** *each node* $v \in V$ **do**
2 store all client flows originating from v in set R_v;
3 normalize bandwidth demands of flows in R_v as $\hat{w}_i = \frac{w_i}{C_{\max}}$, and use it as the size of each flow;
4 use *Algorithm* 2 to classify flows in R_v as small, medium, and largest ones based on their sizes;
5 build an LP to serve medium flows and use *Algorithm* 3 to solve it;
6 serve small and largest flows with *Algorithm* 4;
7 calculate number of used T-Boxes to store in b_v;
8 **end**
9 **return**$(\sum_{v \in V} b_v)$;

1) Flow Classification: To serve the flows originating from each node $v \in V$, we first classify them into a few subsets and label them as small, medium and largest ones with *Algorithm* 2 [22]. *Lines* 1-2 are for the initialization. In *Lines* 3-11, we first check each flow $r_i \in R_v$, and define its color as d_i (*i.e.*, flows to the same destination node have the same color). Then, if the flow's size $\hat{w}_i$ is not larger than the preset tolerance ε, we mark it as a small flow and insert it in set R_v^S (*Line* 6). Otherwise, the flow is inserted in set $R_v^{L,u}$ according to its color (*Lines* 8-9). Next, the for-loop that covers *Lines* 12-22 further divides $R_v^{L,u}$ into $K = \frac{1}{\varepsilon^2}$ subsets. Specifically, if there are at least K flows in $R_v^{L,u}$, we divide it into subsets $\{R_{v,1}^{L,u}, \cdots, R_{v,K}^{L,u}\}$ (*Line* 16), where the size of each subset satisfies

$$\left\lceil |R_v^{L,u}| \cdot \varepsilon^2 \right\rceil = |R_{v,1}^{L,u}| \geq \cdots |R_{v,k}^{L,u}| \geq \cdots \geq |R_{v,K}^{L,u}| = \left\lfloor |R_v^{L,u}| \cdot \varepsilon^2 \right\rfloor. \tag{12}$$

Otherwise, we set $R_{v,1}^{L,u}$ as an empty set, and divide $R_v^{L,u}$ into $K-1$ subsets whose sizes also satisfy Eq. (12) (*Lines* 18-19). Here, for each $u \in V'$, the flows in $R_{v,1}^{L,u}$ have the largest sizes, and thus we mark them as largest ones, while the remaining flows in $\{R_{v,2}^{L,u}, \cdots, R_{v,K}^{L,u}\}$ are labeled as medium ones (*Line* 21). Finally, we set the size of each medium flow as the largest size in its subset with *Lines* 23-27.

2) Serving Medium Flows: Next, we try to serve all the medium flows at first, which can be done by formulating a linear program (LP) and solving it with the PDIP method [23]. For each node $v \in V$, we denote its set of medium flows as

$$R_v^M = \bigcup_{u \in V'} \left(\bigcup_{k=2}^{K} R_{v,k}^{L,u} \right). \tag{13}$$

Algorithm 2: Flow Classification

Input: Set of client flows from node v (R_v) with normalized bandwidths $\{\hat{w}_i\}$, and tolerance ε.
Output: Sets of classified client flows R_v^S and $\{R_{v,k}^{L,u},\ \forall k \in [1, \frac{1}{\varepsilon^2}],\ \forall u \in V'\}$.

1 denote destination set of flows in R_v as $V' = V \setminus v$;
2 $R_v^S = \emptyset$, $\{R_v^{L,u} = \emptyset,\ \forall u \in V'\}$;
3 **for** *each flow* $r_i \in R_v$ **do**
4 define the color of r_i as its destination $d_i \in V'$;
5 **if** $\hat{w}_i \leq \varepsilon$ **then**
6 mark r_i as a small flow and insert it in R_v^S;
7 **else**
8 obtain the color of r_i as $u = d_i$;
9 insert flow r_i in $R_v^{L,u}$;
10 **end**
11 **end**
12 **for** *each node* $u \in V'$ **do**
13 $K = \frac{1}{\varepsilon^2}$;
14 sort flows in $R_v^{L,u}$ in descending order of sizes;
15 **if** $|R_v^{L,u}| \geq K$ **then**
16 partition $R_v^{L,u}$ into $\{R_{v,1}^{L,u}, \cdots, R_{v,K}^{L,u}\}$ in sorted order to satisfy Eq. (12), where $R_{v,1}^{L,u}$ contains the flows with the largest sizes;
17 **else**
18 set $R_{v,1}^{L,u} = \emptyset$;
19 divide $R_v^{L,u}$ into $\{R_{v,2}^{L,u}, \cdots, R_{v,K}^{L,u}\}$ in sorted order to satisfy Eq. (12);
20 **end**
21 mark each $r_i \in R_{v,1}^{L,u}$ as a largest flow, and label the remaining flows in $R_v^{L,u}$ as medium ones;
22 **end**
23 **for** *each node* $u \in V'$ **do**
24 **for** *each* $k \in [2, K]$ **do**
25 set sizes of all flows in $R_{v,k}^{L,u}$ as $\max_{r_i \in R_{v,k}^{L,u}} (\hat{w}_i)$;
26 **end**
27 **end**
28 **return**(R_v^S and $\{R_{v,k}^{L,u},\ \forall k \in [1, \frac{1}{\varepsilon^2}],\ \forall u \in V'\}$);

Before formulating the LP to serve all the flows in R_v^M, we need to clarify the definitions of "flow type" and "allocation mode" since they are the key concepts for understanding it.

Definition 1. *Since all the flows in* $R_{v,k}^{L,u}$ *have the same size after* Algorithm *2, we denote their size as* $\tilde{w}_{v,k}^u$. *Hence, we define* ***the type of each flow*** *in* $R_{v,k}^{L,u}$ *as the tuple* $(\tilde{w}_{v,k}^u, u)$. *We denote the set of flow types as* F_T.

Definition 2. *An* ***allocation mode*** m *is a possible assignment of certain flows in* R_v^M *to a T-Box, which includes* $|F_T| + 1$ *components. In the first* $|F_T|$ *components, the* j*-th one represents the number of type-*j *flows* ($j \in [1, |F_T|]$) *that are allocated to the T-Box. As each T-Box consists of* T *BV-Ts, the flows allocated to the T-Box cannot have more than* T *colors. Hence, the last component of* m *represents the set of the colors of the flows that are assigned to the T-Box, and we*

denote the component as $Dest(m)$.

Since R_v^M is known, we can obtain all the feasible allocation modes to assign certain medium flows in it to a T-Box and store them in set $\mathcal{M}$, based on which the LP is formulated as

Notations:

- $\mathcal{M}$: the set of allocation modes, where each $m \in \mathcal{M}$ represents a feasible allocation mode to assign certain medium flows to a T-Box.
- F_T: the set of flow types.
- $k_{j,m}$: the number of type-j flows ($j \in [1, |F_T|]$), which are assigned in allocation mode $m \in \mathcal{M}$.
- k_j: the total number of type-j flows in R_v^M.

Variables:

- γ_m: the nonnegative integer variable that indicates the number of T-Boxes that serve flows according to allocation mode m, in the final network planning for R_v^M.
- $\delta_{u,\hat{V}}$: the nonnegative real variable that indicates the bandwidth reserved for small flows with color u in a T-Box, which uses an allocation mode m satisfying $Dest(m) = \hat{V}$, where $\hat{V}$ is a subset of V' that includes T colors, and u is a color in $\hat{V}$.

Objective:

The optimization objective of the LP is still to minimize the total number of used T-Boxes.

$$\text{Minimize} \quad \sum_{m \in \mathcal{M}} \gamma_m. \tag{14}$$

Constraints:

$$\sum_{m \in \mathcal{M}} k_{j,m} \cdot \gamma_m \geq k_j, \quad \forall j \in [1, |F_T|]. \tag{15}$$

Eq. (15) ensures that all the flows in R_v^M are served.

$$\sum_{\{m: Dest(m) = \hat{V}\}} \left(1 - \sum_{j=1}^{|F_T|} k_{j,m} \cdot \tilde{w}_j\right) \cdot \gamma_m \geq \sum_{u \in \hat{V}} \delta_{u,\hat{V}}, \quad \{\hat{V} : \hat{V} \subseteq V',\ |\hat{V}| = T\}, \tag{16}$$

$$\sum_{\{\hat{V}: \hat{V} \subseteq V',\ |\hat{V}| = T\}} \delta_{u,\hat{V}} \geq \sum_{\{r_i: r_i \in R_v^S, d_i = u\}} \hat{w}_i, \quad \forall u \in V'. \tag{17}$$

Eqs. (16)-(17) ensure that the bandwidths reserved in all the T-Boxes are enough for serving the small flows in R_v^S, where the $\tilde{w}_j$ in Eq. (16) denotes the size of type-j medium flows.

$$\gamma_m \geq 0, \quad \forall m \in \mathcal{M}, \tag{18}$$

$$\delta_{u,\hat{V}} \geq 0, \quad \forall u \in \hat{V},\ \{\hat{V} : \hat{V} \subseteq V',\ |\hat{V}| = T\}. \tag{19}$$

Eqs. (18)-(19) ensure that the variables are nonnegative.

As the LP above is formulated based on allocation modes, the number of variables in it takes a polynomial form. Hence, the LP can be solved in polynomial-time with the PDIP method [23]. *Algorithm* 3 shows the detailed procedure.

Algorithm 3: Solving the LP to Serve Medium Flows

```
1  transform the LP into the standard form [52], whose
   total number of variables is denoted as N;
2  get the dual problem of the LP;
3  obtain the Karush-Kuhn-Tucker (KKT) condition [53]
   for the primal-dual problem;
4  define a "duality measure" μ to check the gap to the
   optimal solution;
5  while μ ≥ ε/N do
6      solve the nonlinear optimization constructed with
       the Jacobian matrix of the KKT condition for the
       primary-dual problem;
7      use the obtained solution X to update μ;
8  end
9  convert X to the solution of the LP: {γ*_m, δ_{u,V̂}};
10 γ_m = ⌈γ*_m⌉;
11 return({γ_m, δ_{u,V̂}});
```

3) Serving Small and Largest Flows: Finally, we design *Algorithm* 4 to serve the small and largest flows based on the network planning for the medium ones. Here, for node $v \in V$, the set of largest flows can be obtained as

$$R_v^L = \bigcup_{u \in V'} R_{v,1}^{L,u}. \tag{20}$$

In *Lines* 1-3, we allocate a new T-Box to serve each largest flow in R_v^L. Next, the for-loop covering *Lines* 4-11 tries to serve small flows with the remaining bandwidths in the T-Boxes that have been allocated to carry medium flows by *Algorithm* 3. Finally, if there are still unserved small flows, we allocate new T-Boxes to serve them (*Lines* 12-14).

4) Complexity Analysis and Approximation Ratio: It is easy to verify that *Algorithms* 2 and 4 are polynomial-time, and the time complexity of the overall procedure in *Algorithm* 1 is dominated by that of the PDIP method in *Algorithm* 3. Meanwhile, we know that the PDIP method can be accomplished in polynomial-time [23]. Therefore, *Algorithm* 1 is a polynomial-time algorithm to solve the cross-layer planning for FlexE-over-EON in the single-hop scenario.

Algorithm 2 ensures that the number of flow types for the medium flows in R_v^M is at most $|V'| \cdot (\frac{1}{\varepsilon^2} - 1)$, and for any flow in $R_{v,k}^{L,u}$ ($k \geq 2$), its new size $\tilde{w}_{v,k}^u$ will not be greater than the original size of any flow in $R_{v,k-1}^{L,u}$. Hence, if we define the optimal solution of flow set R as $OPT(R)$, we have

$$OPT(R_v^M) \leq OPT(R_v). \tag{21}$$

Next, the performance of the PDIP method in *Algorithm* 3 guarantees that its solution $\{\gamma_m,\ m \in \mathcal{M}\}$ satisfies [23]

$$\sum_{m \in \mathcal{M}} \gamma_m \leq (1 + \varepsilon) \cdot OPT(R_v^M) + (|F_T| + |V'| + |V'|^T), \tag{22}$$

where ε is the preset tolerance and $(|F_T| + |V'| + |V'|^T)$ is a constant. We then consider the largest flows in R_v^L. Note that, the operation principle of the cross-layer planning ensures

$$\sum_{r_i \in R_v^M} \hat{w}_i \leq OPT(R_v^M). \tag{23}$$

Algorithm 4: Serving the Small and Largest Flows

Input: Set of largest flows R_v^L, set of small flows R_v^S, and the solution of *Algorithm* 3: $\{\gamma_m, \delta_{u,\hat{V}}\}$.
Output: Number of additional T-Boxes.

1 **for** *each largest flow* $r_i \in R_v^L$ **do**
2 assign r_i to a new T-Box (dedicated to it only);
3 **end**
4 **for** *each used allocation mode* m *based on* $\{\gamma_m\}$ **do**
5 $\hat{V} = Dest(m)$;
6 calculate remaining bandwidth in the T-Box that uses m as σ_m;
7 **for** *each color* $u \in \hat{V}$ **do**
8 calculate the remaining bandwidth for small flows with color u as $\sigma_{m,u}$;
9 assign unserved small flows with color u to the current T-Box greedily in descending order of their sizes until $\sigma_{m,u}$ is used up;
10 **end**
11 **end**
12 **for** *each color* $u \in \hat{V}$ **do**
13 allocate new T-Boxes and assign unserved small flows with color u (if there are any) to them;
14 **end**
15 **return**(Number of additional T-Boxes);

Meanwhile, for each $u \in V'$, we have

$$|R_{v,1}^{L,u}| \leq 3\varepsilon^2 \cdot |R_v^{L,u} \setminus R_{v,1}^{L,u}| \leq 3\varepsilon \cdot \sum_{r_i \in (R_v^{L,u} \setminus R_{v,1}^{L,u})} \hat{w}_i, \quad (24)$$

as long as we have $\varepsilon \leq \frac{1}{3}$. Therefore, by adding up the two sides of the inequality in Eq. (24), we have

$$|R_v^L| \leq 3\varepsilon \cdot \sum_{r_i \in R_v^M} \hat{w}_i \leq 3\varepsilon \cdot OPT(R_v^M). \quad (25)$$

Hence, based on *Lines* 1-3 in *Algorithm* 4, we can conclude that the number of the additional T-Boxes caused by the largest flows in R_v^L is upper-bounded by $3\varepsilon \cdot OPT(R_v^M)$. Finally, we consider the small flows in R_v^S. The LP solved by *Algorithm* 3 ensures that the bandwidth reserved for small flows with color u in a T-Box, which uses an allocation mode m satisfying $Dest(m) = \hat{V}$ and $u \in \hat{V}$, is at least $\delta_{u,\hat{V}}$. This suggests that for each $m \in \mathcal{M}$ and $u \in Dest(m)$, there is at most one small flow that has not been served after *Line* 11 of *Algorithm* 4. Consequently, with the condition that the size of any small flow will not be greater than ε, we can conclude that the additional bandwidths for these small flows are at most

$$T \cdot \varepsilon \cdot \sum_{m \in \mathcal{M}} \gamma_m^* \leq T \cdot \varepsilon \cdot (1+\varepsilon) \cdot OPT(R_v^M) \leq 2T \cdot \varepsilon \cdot OPT(R_v^M), \quad (26)$$

where γ_m^* denotes the exact solution to the LP. Hence, the number of additional T-Boxes for these small flows is at most

$$\frac{2T \cdot \varepsilon \cdot OPT(R_v^M)}{1-\varepsilon} + |V'| \leq 3T \cdot \varepsilon \cdot OPT(R_v^M). \quad (27)$$

By summarizing the right sides of the inequalities in Eqs. (22), (25) and (27), we obtain that the total number of T-Boxes is upper-bounded by

$$\varpi = [1 + \varepsilon \cdot (3T+4)] \cdot OPT(R_v^M) + (|F_T| + |V'| + |V'|^T), \quad (28)$$

which leads to an approximation ratio of

$$\frac{\varpi}{OPT(R_v)} \leq \frac{\varpi}{OPT(R_v^M)} = [1 + \varepsilon \cdot (3T+4)] + \left(\frac{|F_T| + |V'| + |V'|^T}{OPT(R_v^M)}\right), \quad (29)$$

according to Eq. (21). To this end, we verify that *Algorithm* 1 is a polynomial-time approximation algorithm.

C. Heuristic Algorithm for Single-Hop Scenario

For the performance comparisons in Section VI, we still need a heuristic for the single-hop scenario. However, as the cross-layer planning in FlexE-over-EONs has not been studied in the literature, we cannot directly adopt an existing heuristic. Therefore, we leverage the idea in [9] to design a greedy-based heuristic, as shown in *Algorithm* 5. Specifically, the heuristic serves all the client flows in R sequentially in the greedy manner, using the outer for-loop (*Lines* 1-15). For each flow $r_k \in R$, we first try to leverage a used T-Box in its source s_k to transmit it to d_k (*Lines* 3-11). If this fails, we allocate a new T-Box in s_k to serve r_k (*Line* 12-14). We can easily verify that *Algorithm* 5 is also a polynomial-time algorithm. Nevertheless, it can only provide feasible solutions, but cannot guarantee bounded performance gaps to the optimal solutions.

Algorithm 5: Heuristic for Single-Hop Scenario

Input: Physical topology $G(V, E)$, set of client flows R, and capacity of a T-Box $C_{\max}$.
Output: Total number of used T-Boxes.

1 **for** *each flow* $r_k \in R$ **do**
2 $flag = 0$;
3 **for** *each used T-Box* t *in source node* s_k **do**
4 **if** $flag = 0$ **then**
5 **if** *T-Box* t *has enough capacity to support* w_k *and one of its BV-Ts goes to* d_k **then**
6 $flag = 1$;
7 assign r_k to t and update its capacity;
8 **break**;
9 **end**
10 **end**
11 **end**
12 **if** $flag = 0$ **then**
13 allocate a new T-Box in s_k to serve r_k and connect a BV-T in it to d_k;
14 **end**
15 **end**
16 **return**(Total number of used T-Boxes);

V. Multi-Hop Scenario

In this section, we consider the multi-hop scenario where each client flow can be routed over multiple lightpaths with O/E/O conversions and de-/re-grooming in intermediate nodes.

We tackle the cross-layer planning for the multi-hop scenario with a two-step approach. Specifically, we first solve the virtual topology design to plan the smallest number of lightpaths for carrying all the client flows with multi-hop routing, and then map the client flows in each node to T-Boxes with *Algorithm* 1. Therefore, the focus of this section is the virtual topology design, which can be modeled with the common flow-based ILP in Appendix A. We propose a polynomial-time approximation algorithm to solve the ILP, and for performance evaluations, we also design a greedy-based heuristic for handling the multi-hop scenario with one algorithm.

Note that, different from the single-hop scenario, the two-step approach does not tackle the cross-layer planning with only one optimization. This can make it lose certain optimality. More precisely, because we divide the original problem into two optimizations, a lower bound cannot be computed in the procedure, and thus we cannot obtain the approximation ratio analytically. However, as we design the optimizations in the two steps to work coordinately and propose approximation algorithms for the optimizations in both steps, the performance of the overall cross-layer planning can be maintained well. We will verify this with the simulations in Section VI.

A. Approximation Algorithm for Virtual Topology

Previous studies have already verified that the virtual topology design in network planning is an $\mathcal{NP}$-hard problem [38, 42]. Therefore, we also restore to design a polynomial-time approximation algorithm for it. Specifically, we design the approximation algorithm by leveraging the well-known branch-and-bound method [26], and fix the number of iterations to get a modified branch-and-bound (MBB) approach. By doing so, the proposed algorithm can obtain a qualified solution in polynomial-time. Note that, the MBB approach might not be generalized to all ILP models, and it is applicable to the virtual topology design due to the characteristics of our ILP model.

Algorithm 6 shows the procedure of the MBB-based approximation algorithm. *Lines* 1-3 are for the initialization. Specifically, we relax the ILP for virtual topology design to an LP, solve the LP with the PDIP method whose procedure is similar to that of *Algorithm* 3, and obtain a solution $\{x_{i,j}, y_k^{i,j}\}$ in real numbers. Then, the for-loop covering Lines 4-15 uses I iterations to optimize the solution of the LP. In each iteration, we select the $x_{i,j}$ whose value is the maximum, mark it as processed, and use its value to generate new constraints and get two new LPs $\mathcal{L}_1$ and $\mathcal{L}_2$ (*Lines* 5-8). Then, we solve the new LPs, and utilize the one that provides the smaller objective to update the solution of the original LP (*Lines* 9-14). After the for-loop, *Line* 16 rounds up the real numbers in $\{x_{i,j}, y_k^{i,j}\}$ to get an integer solution. However, since the solution obtained in *Line* 16 is just an approximation one, it might set the value of $y_k^{i,j}$ larger than the correct one, *i.e.*, two routing paths might be assigned to a flow r_k. Hence, we recalculate the routing path of each flow by applying the Dijkstra's algorithm on the designed virtual topology (governed by $\{x_{i,j}\}$), and update $\{y_k^{i,j}\}$ accordingly (*Lines* 17-20).

The time complexity of *Algorithm* 6 is still dominated by that of the PDIP method, and thus it is a polynomial-time

Algorithm 6: MBB-based Virtual Topology Design

Input: Set of nodes V, set of client flows R, preset number of iterations I, and tolerance ε.
Output: Virtual topology design $\{x_{i,j}, y_k^{i,j}\}$.

1 relax the ILP of Eqs. (31)-(39) to get an LP;
2 solve the LP with PDIP method (similar procedure of *Algorithm* 3) to get a solution $\{x_{i,j}, y_k^{i,j}\}$;
3 mark variables $\{x_{i,j},\ \forall i,j\}$ as unprocessed and store them in set X;
4 **for** $n = 1$ *to* I **do**
5 $\quad \hat{x} = \max_{x_{i,j} \in X}(x_{i,j})$, $(i^*, j^*) = \operatorname{argmax}_{x_{i,j} \in X}(x_{i,j})$;
6 $\quad$ mark x_{i^*,j^*} as processed and remove it from X;
7 $\quad$ add a new constraint to the LP: $x_{i^*,j^*} \geq \lfloor \hat{x} \rfloor + 1$, to get a new LP $\mathcal{L}_1$;
8 $\quad$ add a new constraint to the LP: $x_{i^*,j^*} \leq \lfloor \hat{x} \rfloor$, to get another new LP $\mathcal{L}_2$;
9 $\quad$ solve LPs $\mathcal{L}_1$ and $\mathcal{L}_2$ with PDIP method;
10 $\quad$ select LP with smaller objective from $\mathcal{L}_1$ and $\mathcal{L}_2$;
11 $\quad$ denote solution of the chosen LP as $\{\tilde{x}_{i,j}, \tilde{y}_k^{i,j}\}$;
12 $\quad$ **if** *all variables* $\{\lceil \tilde{x}_{i,j} \rceil\}$ *satisfy Eq.* (32) **then**
13 $\quad\quad$ $x_{i,j} = \tilde{x}_{i,j}$, $y_k^{i,j} = \tilde{y}_k^{i,j}$, $\forall i,j,k$;
14 $\quad$ **end**
15 **end**
16 $x_{i,j} = \lceil x_{i,j} \rceil$, $y_k^{i,j} = \lceil y_k^{i,j} \rceil$, $\forall i,j,k$;
17 **for** *each* $r_k \in R$ **do**
18 $\quad$ run the Dijkstra's algorithm in the designed virtual topology for r_k to finalize its routing path;
19 $\quad$ update $\{y_k^{i,j}\}$ accordingly;
20 **end**
21 **return**($\{x_{i,j}, y_k^{i,j}\}$);

algorithm. Based on the principle of the MBB-based approach, we can get the approximation ratio of *Algorithm* 6 as [26]

$$(1+\varepsilon) + \left[\frac{|V| \cdot (|V|-1)}{OPT}\right], \tag{30}$$

where OPT is the objective of the optimal solution. With the virtual topology designed in *Algorithm* 6, we can use the values of $\{y_k^{i,j}\}$ to easily transform the multi-hop scenario to the single-hop one. Then, the cross-layer planning can be solved with the algorithms developed in Section IV.

B. Heuristic Algorithm for Multi-Hop Scenario

Similar to the case for the single-hop scenario, we also design a greedy-based heuristic for the multi-hop scenario. *Algorithm* 7 shows its procedure. For each flow $r_k \in R$, we first try to transmit it directly to d_k with an end-to-end lightpath that originates from a used T-Box in its source s_k (*Lines* 3-11). If this fails, we then try to calculate a multi-hop path with the used T-Boxes in the FlexE-over-EON to route the flow (*Lines* 13-15). But if the path still cannot be found, we allocate a new T-Box in s_k to transmit r_k to d_k with an end-to-end lightpath (*Line* 17). *Algorithm* 7 is also a polynomial-time algorithm without any performance guarantee.

Algorithm 7: Heuristic for Multi-Hop Scenario

Input: Set of nodes V, set of client flows R, and capacity of a T-Box $C_{\max}$.
Output: Total number of used T-Boxes.

for *each flow* $r_k \in R$ **do**
  $flag = 0$;
  for *each used T-Box* t *in source node* s_k **do**
    if $flag = 0$ **then**
      if *T-Box* t *has enough capacity to support* w_k *and one of its BV-Ts goes to* d_k **then**
        $flag = 1$;
        assign r_k to t and update its capacity;
        break;
      end
    end
  end
  if $flag = 0$ **then**
    find a routing path based on used T-Boxes in the FlexE-over-EON to serve r_k;
    if *the path can be found* **then**
      serve r_k with the used T-Boxes on the path and update their capacities;
    else
      allocate a new T-Box in s_k to serve r_k and connect a BV-T in it to d_k;
    end
  end
end
return(Total number of used T-Boxes);

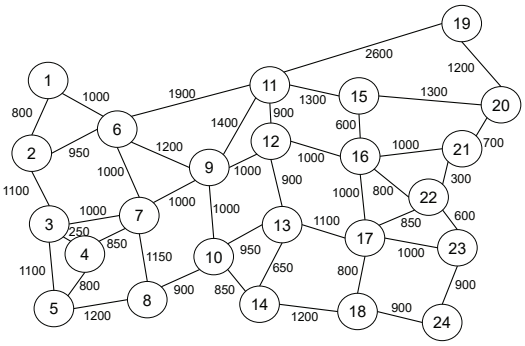

Fig. 3. US Backbone topology.

VI. Simulation Results

In this section, we perform simulations to evaluate the performance of our algorithms for cross-layer network planning.

A. Simulation Setup

The simulations consider both the single-hop and multi-hop scenarios. For the single-hop scenario, we compare the results of the MILP model in Section IV-A to those of *Algorithm* 1. Since the client flows originating from different nodes can be handled independently in the single-hop scenario, we use the 24-node US Backbone (USB) topology in Fig. 3 as the physical topology. Regarding the multi-hop scenario, we first

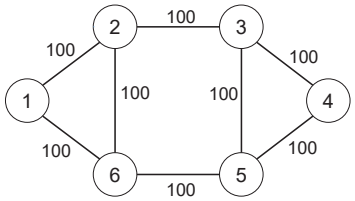

Fig. 4. Six-node topology.

compare the performance of the ILP in Appendix A and *Algorithm* 6 on virtual topology design. Because the ILP will become intractable for a relatively large topology, we only simulate them with the six-node topology in Fig. 4. Then, we evaluate the combination of approximation algorithms (*i.e.*, *Algorithms* 1 and 6) and the heuristic (*Algorithm* 7) to see their overall performance on the cross-layer planning in the multi-hop scenario, using the USB topology in Fig. 3.

We select the bandwidth demands of client flows from $\{10, 40, 25 \cdot \lambda\}$ Gbps, where λ is the bit-rate update multiplier of MAC interfaces [7, 9] and its value is normally within $[1, 8]$. To study the performance of cross-layer planning for different traffic distributions, the simulations consider three scenarios

- *Random Traffic*: bandwidth demands are randomly selected from $\{10, 40, 25 \cdot \lambda\}$ Gbps, where we have $\lambda \in [1, 8]$.
- *Light Traffic*: bandwidth demands are randomly selected from $\{10, 40, 25 \cdot \lambda\}$ Gbps, where we have $\lambda \in [1, 4]$.
- *Heavy Traffic*: bandwidth demands are randomly selected from $\{10, 40, 25 \cdot \lambda\}$ Gbps, where we have $\lambda \in [5, 8]$.

The source-destination pair of each flow is randomly selected. We assume that each T-Box includes $B = 2$ BV-Ts, the capacity of a PHY is $C_p = 100$ Gbps, the maximum capacity of a T-Box is $C_{\max} = 400$ Gbps, and the capacity granularity of each BV-T is $C_g = 12.5$ Gbps. In order to ensure the statistical accuracy of simulation results, we run each simulation with 10 independent sets of client flows, and average the results to obtain each data point. All the simulations are conducted on a computer with 1.6 GHz Inter Core i5-8250 CPU and 8 GB memory, and the simulation environment is MATLAB 2019a with Gurobi optimization toolbox.

B. Single-Hop Scenario

For the single-hop scenario, we first generate $|R| \in \{100, 200, 300, 400\}$ client flows in the 24-node USB, and use the MILP and *Algorithm* 1 to solve the cross-layer planning. Here, we set $\varepsilon = \frac{1}{4}$ in *Algorithm* 1, and select the number of T-Boxes in each node (T) according to $|R|$. For instance, we set $T = 6$ for $|R| = 400$. Table I shows the simulation results for the three traffic scenarios, where "Average T-Boxes" refers to the average number of used T-Boxes per node. We can see that the numbers of used T-Boxes from the MILP are always smaller than those from *Algorithm* 1, while the gaps between the results from the MILP and *Algorithm* 1 always satisfy the approximation ratio in Eq. (29). In the meantime, the results in Table I clearly indicate the advantage of our approximation algorithm in terms of time complexity. For $|R| = 400$ client flows, the running time of the MILP in heavy traffic is more than 7 hours, but that of *Algorithm* 1 is less than 0.4 second.

TABLE I
PERFORMANCE OF MILP AND *Algorithm* 1 FOR SINGLE-HOP SCENARIO

$\|R\|$	Random Traffic				Light Traffic				Heavy Traffic			
	MILP		*Algorithm* 1		MILP		*Algorithm* 1		MILP		*Algorithm* 1	
	Average T-Boxes	Running Time (s)	Average T-Boxes	Running Time (s)	Average T-Boxes	Running Time (s)	Average T-Boxes	Running Time (s)	Average T-Boxes	Running Time (s)	Average T-Boxes	Running Time (s)
100	1.52	6.50	1.81	0.08	1.28	6.26	1.97	0.06	1.69	6.74	2.13	0.09
200	2.49	9.33	2.97	0.16	1.91	7.11	2.57	0.11	2.98	9.85	3.68	0.18
300	3.60	16.19	4.06	0.24	2.32	10.97	3.15	0.17	4.14	59.46	4.99	0.24
400	4.44	32.61	4.97	0.25	2.73	18.40	3.69	0.19	5.35	27685.35	5.90	0.36

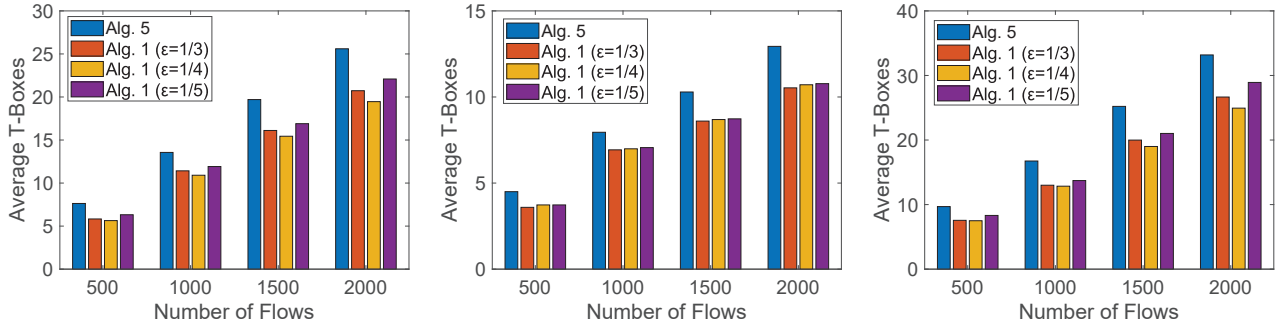

(a) Random Traffic (b) Light Traffic (c) Heavy Traffic

Fig. 5. Large-scale simulation results of *Algorithm* 5 and *Algorithm* 1 for single-hop scenario.

Then, we increase the number of client flows to consider $|R| \in \{500, 1000, 1500, 2000\}$ and further evaluate the performance of *Algorithm* 1. Note that, the MILP has already become intractable for these cases (*i.e.*, it cannot provide the solution within 24 hours). Hence, we only simulate *Algorithm* 1 with ε from $\{\frac{1}{3}, \frac{1}{4}, \frac{1}{5}\}$ and *Algorithm* 5. We still select T based on $|R|$ (*e.g.*, $T = 40$ for $|R| = 2000$), and still consider the three traffic scenarios. Fig. 5 shows the results, which indicate that *Algorithm* 1 with $\varepsilon = \frac{1}{4}$ outperforms those with $\varepsilon \in \{\frac{1}{3}, \frac{1}{5}\}$ in the random and heavy traffic scenarios, while in the light traffic scenario, the one with $\varepsilon = \frac{1}{3}$ uses the least T-Boxes. This suggests that for *Algorithm* 1, the selection of ε should be empirical according to the actual traffic distribution.

We observe that for all the simulation scenarios, *Algorithm* 1 (the approximation algorithm) outperforms *Algorithm* 5 (the heuristic) in terms of the average number of T-Boxes required in the cross-layer planning. This confirms that our approximation algorithm plans FlexE-over-EONs more cost-efficiently than a greedy-based heuristic. The running time of the two algorithms for the problems, whose scales are the largest in the simulations (*i.e.*, $|R| = 2000$), is listed in Table II. We can see that the running time of *Algorithm* 1 decreases with ε. This is because with a smaller ε, the iterations in *Algorithm* 3 take longer time. Because *Algorithm* 5 is just a greedy-based heuristic that does not use iterative optimization, it runs much faster than *Algorithm* 1. Therefore, the approximation algorithm sacrifices running time for the cost-efficiency of cross-layer planning. Note that, our problem is for static network planning, which should be solved in the offline manner before the FlexE-over-EON is actually built. Hence, the running time of network planning algorithms will not be a serious issue. In other words, the network operator is willing to spend more time on network planning, as long as the used algorithm is not intractable and can achieve a significant saving on the capital expenditure (CAPEX).

TABLE II
RUNNING TIME OF ALGORITHMS FOR SINGLE-HOP SCENARIO

Running Time (s)				
$\|R\| = 2000$	*Algorithm* 1	$\varepsilon = \frac{1}{3}$	$\varepsilon = \frac{1}{4}$	$\varepsilon = \frac{1}{5}$
		1.94	9.71	230.87
	Algorithm 5	0.01		

C. Multi-Hop Scenario

In the multi-hop scenario, the cross-layer planning needs to solve two problems, of which the first one is the virtual topology design of the underlying EON, and the second one is just the network planning in the single-hop scenario. Therefore, we tackle the cross-layer planning with a two-step approach. For the first problem (*i.e.*, the virtual topology design), we design both an ILP model and a polynomial-time approximation algorithm (*Algorithm* 6). Hence, the simulations first compare the ILP and *Algorithm* 6, and due to the time complexity of the ILP, they only consider the six-node topology in Fig. 4. Then, in order to evaluate the overall performance of our two-step approach in the multi-hop scenario, we run simulations with a large-scale topology (*i.e.*, the 24-node USB in Fig. 3) to compare the combination of approximation algorithms (*Algorithms* 1 and 6) and the heuristic (*Algorithm* 7).

In the simulations that compare the performance of the ILP and *Algorithm* 6, we generate $|R| \in \{50, 100, 150, 200\}$ client flows, and select the iteration number as $I = |V| \cdot (|V| - 1)$

TABLE III
PERFORMANCE OF ILP AND *Algorithm* 6 FOR VIRTUAL TOPOLOGY DESIGN

$\|R\|$	Random Traffic				Light Traffic				Heavy Traffic			
	ILP		*Algorithm* 6		ILP		*Algorithm* 6		ILP		*Algorithm* 6	
	Average VLs	Running Time (s)	Average VLs	Running Time (s)	Average VLs	Running Time (s)	Average VLs	Running Time (s)	Average VLs	Running Time (s)	Average VLs	Running Time (s)
50	18.80	5.80	20.50	5.74	12.40	20.42	14.20	5.08	19.00	12.87	22.00	5.88
100	29.20	72.88	34.60	9.94	17.00	62.42	21.60	9.21	35.40	361.08	37.80	10.59
150	39.80	145.93	46.00	20.26	23.20	74.46	25.60	20.55	49.40	532.49	57.00	24.87
200	53.20	442.06	60.60	32.65	29.20	371.81	34.40	31.32	63.00	2165.31	70.60	35.98

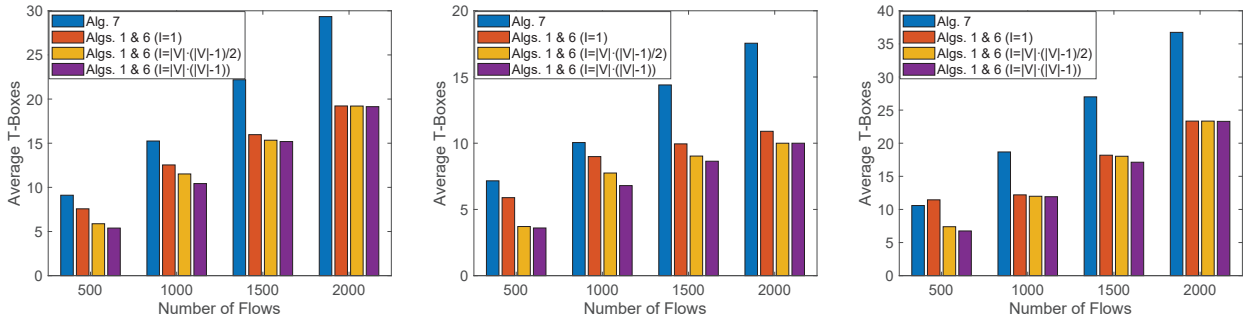

(a) Random Traffic (b) Light Traffic (c) Heavy Traffic

Fig. 6. Large-scale simulation results of *Algorithms* 1 & 6 ($\varepsilon = \frac{1}{4}$) and *Algorithm* 7 for multi-hop scenario.

in *Algorithm* 6. The other parameters are the same as those in the simulations for the single-hop scenario. Table III illustrates the results for the three traffic scenarios, where "Average VLs" refers to the average number of planned lightpaths (*i.e.*, virtual links (VLs)) in the virtual topology. We observed that the numbers of planned lightpaths from the ILP are always smaller than those from *Algorithm* 6, while the gaps between the results from the MILP and *Algorithm* 1 always satisfy the approximation ratio in Eq. (30). Meanwhile, Table IV also verifies the advantage of our approximation algorithm on time complexity. For $|R| = 200$ client flows, the running time of the ILP in heavy traffic is more than half an hour, but that of *Algorithm* 6 is only around 35 seconds.

Next, we evaluate the performance of our two-step approach for the overall cross-layer planning in the multi-hop scenario. This time, we consider $|R| \in \{500, 1000, 1500, 2000\}$ in the 24-node USB. Note that, both the MILP and ILP have become intractable in these cases, and thus we only simulate the combination of approximation algorithms (*Algorithms* 1 and 6) and the heuristic (*Algorithm* 7). For the approximation algorithms, we set $\varepsilon = \frac{1}{4}$, and $I \in \{1, \frac{|V|}{2} \cdot (|V|-1), |V| \cdot (|V|-1)\}$. The simulations still consider the three traffic scenarios. Fig. 6 shows the simulation results, which indicate that when the number of flows increases, the advantage of *Algorithms* 1 and 6 over *Algorithm* 7 becomes more and more obvious, and for the combination of approximation algorithms, the gaps between the results obtained with different values of I gradually decrease. The algorithms' running time for the largest problems (*i.e.*, $|R| = 2000$) is listed in Table IV. We observe that *Algorithms* 1 and 6 with $I = 1$ take less than 12 minutes to accomplish the whole optimization, while if we increase I to $|V| \cdot (|V|-1)$, it will take around 3 hours.

Considering the fact that for these problems, *Algorithms* 1 and 6 do not provide significant different results with $I = 1$ and $I = |V| \cdot (|V|-1)$, we can conclude that using a small value of I is sufficient for the combination of approximation algorithms to handle large-scale problems. The heuristic (*Algorithm* 7) takes shorter running time, but as shown in Fig. 6, its solutions are much less cost-efficient than those from *Algorithms* 1 and 6. Once again, as our problem is for static network planning, the operator will pay much more attention on the CAPEX of required equipment.

TABLE IV
RUNNING TIME OF ALGORITHMS FOR MULTI-HOP SCENARIO

Running Time (s)			
$\|R\| = 2000$	*Algorithms* 1 & 6	$\varepsilon = \frac{1}{4}$	
		$I = 1$	$I = \|V\| \cdot (\|V\|-1)$
		697.39	10573.30
	Algorithm 7	0.26	

VII. CONCLUSION

In this paper, we studied the problem of cross-layer network planning for FlexE-over-EONs, and focused our problem-solving on the FlexE-over-EONs based on the FlexE-aware architecture. We first considered the single-hop scenario in which all the client flows are assumed to be routed over end-to-end lightpaths in the EON. We proved that the cross-layer planning for this scenario can be transformed into CCBP, and proposed a polynomial-time approximation algorithm to solve it based on the PDIP method. Next, we expanded our study to address a more realistic multi-hop scenario, where each

client flow can be routed over multiple lightpaths in the EON. We formulated the virtual topology design in the scenario as an ILP model, and then also designed a polynomial-time approximation algorithm based on MBB. With the virtual topology designed, we obtained the hop-by-hop lightpath routing of each client flow, and transformed the cross-layer planning to that of the single-hop scenario. To evaluate the performance of our two-step method for the multi-hop scenario, we also proposed a heuristic algorithm. Extensive simulations confirmed that regarding large-scale cross-layer planning for FlexE-over-EONs, our approximation algorithms outperform the ILP/MILP models significantly in terms of running time, their gaps to the optimal solutions are guaranteed, and their solutions are much better than those from the heuristic.

Appendix A
ILP Model for Virtual Topology Design

As the physical topology $G(V, E)$ is definitely a connected graph to ensure feasible cross-layer network planning, the virtual topology design does not need to care too much about the physical links. Hence, we number the nodes in V with indices in $[1, |V|]$, and refer to each node with its index.

Notations:

- V: the set of nodes in the physical topology, and each node is referred to with its index $i \in [1, |V|]$.
- R: the set of client flows, where r_k is the k-th flow, with a bandwidth demand of w_k in Gbps and a source-destination pair as s_k-d_k.
- T: the number of T-Boxes in each node.
- $C_{\max}$: the maximum capacity of a lightpath (*i.e.*, $C_{\max}$ can be obtained with Eq. (11)).

Variables:

- $x_{i,j}$: the nonnegative integer variable that indicates the number of directed lightpaths from node i to node j.
- $y_k^{i,j}$: the boolean variable that equals 1 if flow r_k uses a directed lightpath from node i to node j, and 0 otherwise.

Objective:

The optimization objective is to minimize the total number of lightpaths planned in the virtual topology.

$$\text{Minimize} \quad \sum_{i,j \in [1,|V|]} x_{i,j}. \tag{31}$$

Constraints:

$$\sum_{j \in [1,|V|]} x_{i,j} \le T, \quad \forall i \in [1, |V|]. \tag{32}$$

Eq. (32) ensures that the number of planned lightpaths does not exceed the number of T-Boxes in each node.

$$y_k^{i,j} \le x_{i,j}, \quad \forall r_k \in R,\ i \in [1, |V|],\ j \in [1, |V|]. \tag{33}$$

Eq. (33) ensures that flows will not be assigned to nonexistent lightpaths.

$$\sum_{j \in [1,|V|]} y_k^{s_k,j} = 1, \quad \forall r_k \in R. \tag{34}$$

Eq. (34) ensures that each flow is assigned to one and only one lightpath that is from its source.

$$\sum_{i \in [1,|V|]} y_k^{i,d_k} = 1, \quad \forall r_k \in R. \tag{35}$$

Eq. (35) ensures that each flow is assigned to one and only one lightpath that is ended at its destination.

$$\sum_{i \in [1,|V|]} y_k^{i,l} = \sum_{j \in [1,|V|]} y_k^{l,j}, \quad \forall r_k \in R, \\ \{l : l \in [1, |V|], l \ne s_k, l \ne d_k\}. \tag{36}$$

Eq. (36) ensures that each flow is handled correctly at the intermediate nodes on its routing path.

$$\sum_{i \in [1,|V|]} y_k^{i,l} \le 1,\ \forall r_k \in R,\ \{l : l \in [1, |V|], l \ne s_k, l \ne d_k\}. \tag{37}$$

Eq. (37) ensures that for each node in the topology, there is at most one lightpath from it, which carries the flow r_k.

$$\sum_{j \in [1,|V|]} y_k^{l,j} \le 1,\ \forall r_k \in R,\ \{l : l \in [1, |V|], l \ne s_k, l \ne d_k\}. \tag{38}$$

Eq. (38) ensures that for each node in the topology, there is at most one lightpath to it, which carries the flow r_k. Note that, Eqs. (33)-(38) are the constraints to ensure flow conservation, *i.e.*, they guarantee that for any flow $r_k \in R$, the routing path from its source to its destination is unique and loopless.

$$\sum_{r_k \in R} y_k^{i,j} \cdot w_k \le x_{i,j} \cdot C_{\max}, \quad \forall r_k \in R,\ i, j \in [1, |V|]. \tag{39}$$

Eq. (39) ensures that the total bandwidth of the flows assigned to each lightpath does not exceed its capacity.

Acknowledgments

This work was supported in part by the NSFC projects 61871357, 61771445 and 61701472, ZTE Research Fund PA-HQ-20190925001J-1, Zhejiang Lab Research Fund 2019LE0AB01, CAS Key Project (QYZDY-SSW-JSC003), and SPR Program of CAS (XDC02070300).

References

[1] "Cisco global cloud index: Forecast and methodology, 2016-2021." [Online]. Available: https://www.cisco.com/c/en/us/solutions/collateral/service-provider/global-cloud-index-gci/white-paper-c11-738085.html.

[2] A. Gupta and R. Jha, "A survey of 5G network: Architecture and emerging technologies," *IEEE Access*, vol. 3, pp. 1206–1232, Aug. 2015.

[3] P. Lu *et al.*, "Highly-efficient data migration and backup for Big Data applications in elastic optical inter-datacenter networks," *IEEE Netw.*, vol. 29, pp. 36–42, Sept./Oct. 2015.

[4] N. Xue *et al.*, "Demonstration of OpenFlow-controlled network orchestration for adaptive SVC video manycast," *IEEE Trans. Multimedia*, vol. 17, pp. 1617–1629, Sept. 2015.

[5] J. Liu *et al.*, "On dynamic service function chain deployment and readjustment," *IEEE Trans. Netw. Serv. Manag.*, vol. 14, pp. 543–553, Sept. 2017.

[6] "FlexE." [Online]. Available: https://en.wikipedia.org/wiki/FlexE.

[7] "Flex Ethernet 2.0 implementation agreement," Optical Internetworking Forum, Jun. 2018. [Online]. Available: https://www.oiforum.com/wp-content/uploads/2019/01/OIF-FLEXE-02.0-1.pdf.

[8] H. Oliveira, I. Katib, N. Fonseca, and D. Medhi, "Comparison of network protection in three-layer IP/MPLS-over-OTN-over-DWDM networks," in *Proc. of GLOBECOM 2015*, pp. 1–6, Dec. 2015.

[9] A. Eira, A. Pereira, J. Pires, and J. Pedro, "On the efficiency of flexible ethernet client architectures in optical transport networks," *J. Opt. Commun. Netw.*, vol. 10, pp. A133–A143, Jan. 2018.

[10] O. Gerstel, M. Jinno, A. Lord, and B. Yoo, "Elastic optical networking: A new dawn for the optical layer?" *IEEE Commun. Mag.*, vol. 50, pp. 12–20, Feb. 2012.

[11] L. Gong *et al.*, "Efficient resource allocation for all-optical multicasting over spectrum-sliced elastic optical networks," *J. Opt. Commun. Netw.*, vol. 5, pp. 836–847, Aug. 2013.

[12] Y. Yin *et al.*, "Spectral and spatial 2D fragmentation-aware routing and spectrum assignment algorithms in elastic optical networks," *J. Opt. Commun. Netw.*, vol. 5, pp. A100–A106, Oct. 2013.

[13] L. Gong and Z. Zhu, "Virtual optical network embedding (VONE) over elastic optical networks," *J. Lightw. Technol.*, vol. 32, pp. 450–460, Feb. 2014.

[14] L. Zhang and Z. Zhu, "Spectrum-efficient anycast in elastic optical inter-datacenter networks," *Opt. Switch. Netw.*, vol. 14, pp. 250–259, Aug. 2014.

[15] M. Jinno *et al.*, "Multiflow optical transponder for efficient multilayer optical networking," *IEEE Commun. Mag.*, vol. 50, pp. 56–65, May 2012.

[16] Z. Zhu *et al.*, "Demonstration of cooperative resource allocation in an OpenFlow-controlled multidomain and multinational SD-EON testbed," *J. Lightw. Technol.*, vol. 33, pp. 1508–1514, Apr. 2015.

[17] N. Sambo *et al.*, "Next generation sliceable bandwidth variable transponders," *IEEE Commun. Mag.*, vol. 53, pp. 163–171, Feb. 2015.

[18] S. Dahlfort, M. Xia, R. Proietti, and S. Yoo, "Split spectrum approach to elastic optical networking," in *Proc. of ECOC 2012*, pp. 1–3, Sept. 2012.

[19] W. Lu *et al.*, "Dynamic multi-path service provisioning under differential delay constraint in elastic optical networks," *IEEE Commun. Lett.*, vol. 17, pp. 158–161, Jan. 2013.

[20] Z. Zhu, W. Lu, L. Zhang, and N. Ansari, "Dynamic service provisioning in elastic optical networks with hybrid single-/multi-path routing," *J. Lightw. Technol.*, vol. 31, pp. 15–22, Jan. 2013.

[21] W. Lu *et al.*, "How much can flexible ethernet and elastic optical networking benefit mutually?" in *Proc. of ICC 2019*, pp. 1–6, May 2019.

[22] L. Epstein, C. Imreh, and A. Levin, "Class constrained bin packing revisited," *Theor. Comput. Sci.*, vol. 411, pp. 3073–3089, Apr. 2010.

[23] J. Nocedal and S. Wright, *Numerical Optimization*. Springer Science & Business Media, 2006.

[24] H. Oliveira and N. Fonseca, "Multipath routing, spectrum and core allocation in protected SDM elastic optical networks," in *Proc. of GLOBECOM 2019*, pp. 1–6, Dec. 2019.

[25] ——, "P-cycle protected multipath routing, spectrum and core allocation in SDM elastic optical networks," in *Proc. of ICC 2019*, pp. 1–6, Jun. 2019.

[26] E. Lawler and D. Wood, "Branch-and-bound methods: A survey," *Oper. Res.*, vol. 14, pp. 699–719, Jan. 1966.

[27] Z. Zhu *et al.*, "Jitter and amplitude noise accumulations in cascaded all-optical regenerators," *J. Lightw. Technol.*, vol. 26, pp. 1640–1652, Jun. 2008.

[28] Z. Pan *et al.*, "Advanced optical-label routing system supporting multicast, optical TTL, and multimedia applications," *J. Lightw. Technol.*, vol. 23, pp. 3270–3281, Oct. 2005.

[29] H. Jiang, Y. Wang, L. Gong, and Z. Zhu, "Availability-aware survivable virtual network embedding (A-SVNE) in optical datacenter networks," *J. Opt. Commun. Netw.*, vol. 7, pp. 1160–1171, Dec. 2015.

[30] L. Gong, H. Jiang, Y. Wang, and Z. Zhu, "Novel location-constrained virtual network embedding (LC-VNE) algorithms towards integrated node and link mapping," *IEEE/ACM Trans. Netw.*, vol. 24, pp. 3648–3661, Dec. 2016.

[31] B. Li, W. Lu, S. Liu, and Z. Zhu, "Deep-learning-assisted network orchestration for on-demand and cost-effective vNF service chaining in inter-DC elastic optical networks," *J. Opt. Commun. Netw.*, vol. 10, pp. D29–D41, Oct. 2018.

[32] K. Christodoulopoulos, I. Tomkos, and E. Varvarigos, "Elastic bandwidth allocation in flexible OFDM-based optical networks," *J. Lightw. Technol.*, vol. 29, pp. 1354–1366, May 2011.

[33] L. Gong, X. Zhou, W. Lu, and Z. Zhu, "A two-population based evolutionary approach for optimizing routing, modulation and spectrum assignments (RMSA) in O-OFDM networks," *IEEE Commun. Lett.*, vol. 16, pp. 1520–1523, Sept. 2012.

[34] M. Zhang, C. You, H. Jiang, and Z. Zhu, "Dynamic and adaptive bandwidth defragmentation in spectrum-sliced elastic optical networks with time-varying traffic," *J. Lightw. Technol.*, vol. 32, pp. 1014–1023, Mar. 2014.

[35] H. Wu, F. Zhou, Z. Zhu, and Y. Chen, "On the distance spectrum assignment in elastic optical networks," *IEEE/ACM Trans. Netw.*, vol. 25, pp. 2391–2404, Aug. 2017.

[36] W. Lu and Z. Zhu, "Dynamic service provisioning of advance reservation requests in elastic optical networks," *J. Lightw. Technol.*, vol. 31, pp. 1621–1627, May 2013.

[37] H. Wu, F. Zhou, Z. Zhu, and Y. Chen, "Analysis framework of RSA algorithms in elastic optical rings," *J. Lightw. Technol.*, vol. 37, pp. 1113–1122, Feb. 2019.

[38] S. Zhang *et al.*, "Evolving traffic grooming in multi-layer flexible-grid optical networks with software-defined elasticity," *J. Lightw. Technol.*, vol. 32, pp. 2905–2914, Aug. 2014.

[39] S. Liu *et al.*, "DL-assisted cross-layer orchestration in software-defined IP-over-EONs: From algorithm design to system prototype," *J. Lightw. Technol.*, vol. 37, pp. 4426–4438, Sept. 2019.

[40] M. Ruiz *et al.*, "Survivable IP/MPLS-over-WSON multilayer network optimization," *J. Opt. Commun. Netw.*, no. 8, pp. 629–640, Mar. 2011.

[41] P. Papanikolaou, K. Christodoulopoulos, and E. Varvarigos, "Joint multi-layer survivability techniques for IP-over-elastic-optical-networks," *J. Opt. Commun. Netw.*, vol. 9, pp. A85–A98, Jan. 2017.

[42] W. Lu, X. Yin, X. Cheng, and Z. Zhu, "On cost-efficient integrated multilayer protection planning in IP-over-EONs," *J. Lightw. Technol.*, vol. 36, pp. 2037–2048, May 2018.

[43] J. Zhang *et al.*, "Dynamic traffic grooming in sliceable bandwidth-variable transponder-enabled elastic optical networks," *J. Lightwave Technol.*, vol. 33, pp. 183–191, Jan. 2015.

[44] F. Tang *et al.*, "Mixed channel traffic grooming for IP over EON with SBPP-based cross-layer protection," *J. Lightwave Technol.*, vol. 35, pp. 3836–3848, Jul. 2017.

[45] S. Liu, W. Lu, and Z. Zhu, "On the cross-layer orchestration to address IP router outages with cost-efficient multilayer restoration in IP-over-EONs," *J. Opt. Commun. Netw.*, vol. 10, pp. A122–A132, Jan. 2018.

[46] J. Zhang *et al.*, "Energy-efficient traffic grooming in sliceable-transponder-equipped IP-over-elastic optical networks," *J. Opt. Commun. Netw.*, vol. 7, pp. 142–152, Jan. 2015.

[47] S. Trowbridge, "Ethernet and OTN: 400G and beyond," in *Proc. of OFC 2015*, pp. 1–3, Mar. 2015.

[48] T. Hofmeister, V. Vusirikala, and B. Koley, "How can flexibility on the line side best be exploited on the client side?" in *Proc. of OFC 2016*, pp. 1–3, Mar. 2016.

[49] A. Patel *et al.*, "Flexible-client: The missing piece towards transport software-defined networks," in *Proc. of OFC 2014*, pp. 1–3, Mar. 2014.

[50] A. Eira and J. Pedro, "How much transport grooming is needed in the age of flexible clients?" in *Proc. of OFC 2017*, pp. 1–3, Mar. 2017.

[51] P. Moura, N. Fonseca, and R. Scaraficci, "Fragmentation aware routing and spectrum assignment algorithm," in *Proc. of ICC 2014*, pp. 1137–1142, Jun. 2014.

[52] N. Karmarkar and R. Karp, "An efficient approximation scheme for the one-dimensional bin-packing problem," in *Proc. of SFCS 1982*, pp. 312–320, Nov. 1982.

[53] S. Boyd and L. Vandenberghe, *Convex Optimization*. Cambridge University Press, 2004.